Weierstraß-Institut
für Angewandte Analysis und Stochastik
Leibniz-Institut im Forschungsverbund Berlin e. V.

Preprint ISSN 2198-5855

A revisited Johnson–Mehl–Avrami–Kolmogorov model and the evolution of grain-size distributions in steel

Dietmar Hömberg[1], Francesco Saverio Patacchini[2],

Kenichi Sakamoto[3], Johannes Zimmer[4]

submitted: August 8, 2016

[1] Weierstrass Institute
Mohrenstr. 39
10117 Berlin
Germany
and
Department of Mathematical Sciences
NTNU
Alfred Getz vei 1
7491 Trondheim
Norway
E-Mail: dietmar.hoemberg@wias-berlin.de

[2] Department of Mathematics
Imperial College London
South Kensington Campus
London SW7 2AZ
UK
E-Mail: fsp13@imperial.ac.uk

[3] Mathematical Science & Technology Research Lab
Advanced Technology Research Laboratories
Technical Development Bureau
Nippon Steel & Sumitomo Metal Corporation
20-1 Shintomi
Futtsu-City, Chiba, 293-8511
Japan
E-Mail: sakamoto.a2c.kenichi@jp.nssmc.com

[4] Department of Mathematical Sciences
University of Bath
Bath BA2 7AY
UK
E-Mail: zimmer@maths.bath.ac.uk

No. 2283
Berlin 2016

2000 *Mathematics Subject Classification.* 35Q84, 35Q74, 35K10, 74H40.

Key words and phrases. Grain size distribution, Fokker-Planck equation, nucleation and growth, phase transitions.

Edited by
Weierstraß-Institut für Angewandte Analysis und Stochastik (WIAS)
Leibniz-Institut im Forschungsverbund Berlin e. V.
Mohrenstraße 39
10117 Berlin
Germany

Fax: +49 30 20372-303
E-Mail: preprint@wias-berlin.de
World Wide Web: http://www.wias-berlin.de/

1. Introduction

Steel is still the most important construction material in industrialised countries. Driven especially by the goal of vehicle weight reduction in automotive industry, the last two decades have seen the development of many new steel grades, such as dual, trip, or twip steels combining both strength and ductility. The production of these new steels requires a precise process guidance [21, 8]. It has turned out that best results are achieved if in addition to temperature measurements, the resulting microstructure is also monitored. Macroscopic phase transition models allowing for a coupling with finite element simulation of temperature evolution have thus gained increasing interest.

A classical model to describe diffusive nucleation and growth is the Johnson-Mehl-Avrami-Kolmogorov (JMAK) model, developed independently by Johnson and Mehl [16], Avrami [1, 2, 3], and Kolmogorov [17]. A review of the JMAK model can be found in [12]. Assuming constant nucleation and growth rates α and ρ, respectively, it states that the volume fraction $P(t)$ at some time t of a new phase growing from a parent phase by a nucleation and growth process is in three dimensions given by

$$P(t) = 1 - \exp\left(-\frac{\pi\alpha\rho^3 t^4}{3}\right). \tag{1.1}$$

This JMAK equation is widely used in engineering literature due to its simplicity; in fact, many extensions of it to situations with non-constant nucleation and growth rates can be found.

The first contribution of this paper is to revisit the classical nucleation and growth modelling approach of the aforementioned authors. Specifically, in Section 2 we focus on the growth of ferrite phase from the high temperature austenite phase, which plays an important role, e.g., in dual phase and trip steels. Ferrite is a solid solution of carbon in face-centred cubic (f.c.c.) iron. Its growth is governed by the diffusion of carbon into the remaining austenite, thereby enriching its carbon content. The transition naturally ceases when the equilibrium fraction of carbon in austenite is reached—this is the so-called *soft impingement*.

An important aim of material simulation is the prediction of mechanical properties. However, especially in heterogeneous materials such as metals, a representative volume (or concentration) approach is not sufficient to predict material properties if it does not account for the distribution of grain (or nucleus) sizes. Furthermore, a macroscopic nucleation and growth model is not capable of resolving mesoscopic grain boundaries. The second contribution of this paper is to gather additional information about the material heterogeneity by studying the grain-size distribution. As shown in [7], this can then be used by a stochastic homogenisation approach to derive mechanical properties.

As a conserved quantity, the grain-size (volume) distribution is governed by a Fokker-Planck equation derived and solved in Section 3. Grain-size distributions in austenite and ferrite are of log-normal type [18], as is the solution to the Fokker-Planck equation we study. For a different application of similar Fokker-Planck models, see for example [10]. In Section 4 we present simulations and a numerical parameter study. In a forthcoming paper, we will discuss parameter identification issues for this Fokker-Planck model and compare it to real-world data. As a preparation, we discuss in Section 5 how volume distributions can be compared with area distributions drawn from polished micrograph sections. For results about the identification of temperature-dependent growth rates exploiting dilatometer experiments, we refer to [14, 13].

The promising feature of this approach is that it allows for an easy calculation of grain-size distributions on a macroscopic level without explicit mesoscopic simulations as in the phase-field approach, opening up at least two interesting and obvious areas of further research. The first one is the inclusion of thermal effects by a spatial two-scale model combining area space with the macroscopic specimen space. The

second one is the use of these grain-size distributions for a computation of homogenised mechanical properties.

It is noteworthy at this point that our approach should not be confused with grain boundary character distribution evolution models of Fokker-Planck type as they have been investigated in a series of papers by Barmak *et al.* (see, e.g., [5, 6] and the references therein). While these authors study *coarsening effects* in polycrystalline solids, i.e., a single phase situation, the present paper is concerned with the evolution of the grain-size distribution during an irreversible phase transition without coarsening. Here, no grain can grow at the expense of others, no grain shrinks, and no grain can grow into others when touching—this is the so-called *hard impingement*. Similarly, the approach taken in this paper for nucleation and growth processes is different from the Becker-Döring type models of coagulating particles or droplets, see, e.g., [4, 20].

2. The revisited JMAK model

Consider a bounded domain $\Omega \subset \mathbb{R}^3$, whose volume is denoted by $V = |\Omega|$, composed exclusively of an austenite phase and a ferrite phase, and where austenite may transform into ferrite as time increases. The sub-volume of austenite present at time t is denoted by $V_{\mathrm{A}}(t)$, and the one of ferrite by $V_{\mathrm{F}}(t)$. By conservation of volume we have $V = V_{\mathrm{A}}(t) + V_{\mathrm{F}}(t)$ for all $t \in [0, T]$, where $T > 0$ is a fixed final time. Then, the volume phase fraction of ferrite is defined by

$$P(t) = \frac{V_{\mathrm{F}}(t)}{V}. \tag{2.1}$$

To derive our model, we assume that the phase transformation happens isothermally at temperature $\theta > 0$, although this can be easily generalised.

We assume that ferrite grains appear randomly in the austenite matrix Ω with nucleation rate $\alpha = \alpha(\theta)$ (number of grains per unit time per unit volume) and grow isotropically, that is as spheres, with growth rate $\rho(t, \theta) = \rho(t)$ (length per unit time). We suppose that when two growing grains touch, these cannot grow into each other, and thus only continue growing towards the "free" directions, which is the hard impingement assumption. After two grains meet, they therefore do not look as spheres anymore, but rather as the union of two intersected spheres. Let us point out that hard impingement also describes the "interaction" between the grains and the boundary of the domain Ω when these touch. In this setting, the volume occupied at time t by an isolated ferrite grain born at time τ is

$$\nu(t, \tau) = \frac{4\pi}{3} \left(\int_\tau^t \rho(s) \, \mathrm{d}s \right)^3. \tag{2.2}$$

Consider an extended volume, denoted by $V^{\mathrm{ext}}(t)$, which is the total volume occupied by all ferrite grains at time t, assuming temporarily that they may grow into each other. This gives, using (2.1),

$$V_{\mathrm{F}}^{\mathrm{ext}}(t) = V\alpha \int_0^t \nu(t, \tau) \, \mathrm{d}\tau.$$

Invoking the Avrami correction (see [1, 2, 3] for a derivation, and also [17]) to incorporate hard impingement, we have

$$V \mathrm{d}P(t) = \mathrm{d}V_{\mathrm{F}}(t) = (1 - P(t)) \, \mathrm{d}V_{\mathrm{F}}^{\mathrm{ext}}(t).$$

By integrating the above equation, using (2.2) and supposing that $P(0) = 0$, we get

$$-\log(1 - P(t)) = \frac{4\pi\alpha}{3} \int_0^t \left(\int_\tau^t \rho(s) \, \mathrm{d}s \right)^3 \mathrm{d}\tau. \tag{2.3}$$

Note that, by assuming that $\rho(t) = \rho$ does not depend on time, and by taking the exponential of both sides of (2.3), we recover (1.1). Equation (2.3) yields

$$\begin{cases} P'(t) = 4\pi\alpha\rho(t)(1-P(t)) \displaystyle\int_0^t \left(\int_\tau^t \rho(s)\,\mathrm{d}s \right)^2 \mathrm{d}\tau, \\ P(0) = 0. \end{cases} \tag{2.4}$$

In order to close the differential equation (2.4), we need now to choose a law for the evolution of the growth rate ρ. This is where we incorporate soft impingement into the model. This means that the transformation ceases naturally when the actual carbon concentration in austenite, $C_{\mathrm{A}}(t)$, reaches the equilibrium value $C_{\mathrm{A}}^{\mathrm{eq}} = C_{\mathrm{A}}^{\mathrm{eq}}(\theta)$, corresponding to an equilibrium volume $V_{\mathrm{F}}^{\mathrm{eq}} = V_{\mathrm{F}}^{\mathrm{eq}}(\theta)$ and equilibrium fraction $P^{\mathrm{eq}} = V_{\mathrm{F}}^{\mathrm{eq}}/V$. Then $C_{\mathrm{A}}(t)$ can be computed from mass conservation by assuming that the carbon concentration in ferrite is constant and equal to its equilibrium value $C_{\mathrm{F}}^{\mathrm{eq}} = C_{\mathrm{F}}^{\mathrm{eq}}(\theta)$ (defined as the carbon concentration in ferrite when $C_{\mathrm{A}}^{\mathrm{eq}}$ is reached), i.e.,

$$C = C_{\mathrm{F}}^{\mathrm{eq}} P(t) + C_{\mathrm{A}}(t)(1-P(t)),$$

where C is the overall carbon concentration in the steel sample Ω. From this it follows that, if $C_{\mathrm{A}}^{\mathrm{eq}} \neq C_{\mathrm{F}}^{\mathrm{eq}}$ (otherwise nothing happens), the equilibrium volume fraction of ferrite satisfies

$$P^{\mathrm{eq}} = \frac{C_{\mathrm{A}}^{\mathrm{eq}} - C}{C_{\mathrm{A}}^{\mathrm{eq}} - C_{\mathrm{F}}^{\mathrm{eq}}} \quad \text{and} \quad \frac{P^{\mathrm{eq}} - P(t)}{1-P(t)} = \frac{C_{\mathrm{A}}^{\mathrm{eq}} - C_{\mathrm{A}}(t)}{C_{\mathrm{A}}^{\mathrm{eq}} - C_{\mathrm{F}}^{\mathrm{eq}}}.$$

We then require the growth rate $\rho(t)$ to be proportional to $C_{\mathrm{A}}^{\mathrm{eq}} - C_{\mathrm{A}}(t)$, and we make the choice

$$\rho(t) = \frac{\rho_*}{ct^\gamma} \frac{P^{\mathrm{eq}} - P(t)}{1-P(t)}, \quad 0 \leq \gamma < 1,$$

where $\rho_* = \rho_*(\theta) > 0$ is some reference growth rate, and c is a constant with the same dimension as $t^{-\gamma}$; for simplicity, we take $c := 1$. The term t^γ allows for the description of time-dependent growth rates, independently of soft impingement. In the case of classical diffusional growth, we have $\gamma = 0.5$. This ansatz for the growth rate then results in the integro-differential equation model

$$P'(t) = 4\pi\alpha\rho_* t^{-\gamma}(P^{\mathrm{eq}} - P(t)) \int_0^t \left(\int_\tau^t \frac{\rho_*}{s^\gamma} \frac{P^{\mathrm{eq}} - P(s)}{1-P(s)}\,\mathrm{d}s \right)^2 \mathrm{d}\tau.$$

Note that the equilibrium value P^{eq} is only reached asymptotically. This equation can be dealt with by transformation to a system of ODEs. To this end, we perform the substitutions

$$z(t,\tau) = \int_\tau^t \rho(s)\,\mathrm{d}s, \quad y(t) = \alpha \int_0^t z(t,\tau)^2\,\mathrm{d}\tau, \quad x(t) = \alpha \int_0^t z(t,\tau)\,\mathrm{d}\tau, \quad w(t) = \alpha t.$$

Altogether we obtain

$$\begin{cases} w'(t) = \alpha, \quad x'(t) = \rho(t)w(t), \quad y'(t) = 2\rho(t)x(t), \\ P'(t) = 4\pi(1-P(t))\rho(t)y(t), \end{cases}$$

with $w(0) = x(0) = y(0) = P(0) = 0$. We can finally introduce the number of grains born until time t per unit volume

$$N(t) = \alpha \int_0^t \left(1 - \frac{P(\tau)}{P^{\mathrm{eq}}} \right) \mathrm{d}\tau. \tag{2.5}$$

The expression above takes soft impingement into account as well by requiring that nucleation stops when P^{eq} is reached.

3. The grain-size distribution model

3.1. **Derivation of the governing equation.** The *volume distribution* of ferrite grains

$$\phi(\nu,t)\colon (0,\infty)\times[t_0,T]\to[0,\infty) \tag{3.1}$$

counts, at time t, the number of grains of volume ν per unit volume, normalised by the total number of grains. This means that, for any $\nu_2 > \nu_1 \geq 0$, the quantity $\int_{\nu_1}^{\nu_2}\phi(\nu,t)\,\mathrm{d}\nu$ is the relative number of grains with volumes in $[\nu_1,\nu_2]$, which implies that $\phi(\cdot,t)$ is a probability density on $(0,\infty)$, that is, $\int_0^\infty \phi(\nu,t)\,\mathrm{d}\nu = 1$. In (3.1), $t_0 > 0$ is a small *incubation* time, before which the notion of volume distribution does not make physical sense (see [22] for an account on the notion of incubation time). Combining this quantity with those of the model derived in Section 2, we get

$$\int_0^\infty \nu\phi(\nu,t)\,\mathrm{d}\nu = \frac{P(t)}{N(t)} =: g(t) \quad \text{for all } t\in[t_0,T], \tag{3.2}$$

where we recall from (2.1) that P is the volume phase fraction of ferrite and the left-hand side is the first moment of $\phi(\cdot,t)$ at time t, i.e., the mean volume of the grains. This equation bridges the meso- and macroscopic scales, giving us another nice feature of the JMAK model, namely that it allows to compute the mean grain size without relying on further mesoscopic information. We refer to [9, 23, 11] for mathematical studies of Fokker-Planck/gradient flow equations with moment constraints.

Since $\phi(\cdot,t)$ has conserved unit mass over all times $t\in[t_0,T]$, we assume that ϕ satisfies the continuity equation $\phi_t + J_\nu = 0$, with

$$J(\nu,t) = \mu_1(\nu,t)\phi - (\mu_2(\nu,t)\phi)_\nu,$$

where the mobility terms μ_1 and μ_2 are assumed to be separable, $\mu_1(\nu,t) = \mu_{11}(t)\mu_{12}(\nu)$ and $\mu_2(\nu,t) = \mu_{21}(t)\mu_{22}(\nu)$. Here, we suppose that $\mu_{12}(\nu) = \nu$ and $\mu_{22}(\nu) = \nu^2$. These choices are justified *a posteriori*: they allow the derivation of an explicit solution for the volume distribution which is log-normally distributed (see Section 3.2); and this log-normal behaviour is experimentally observed. Also, we write $v(t) := \mu_{11}(t)$ and $\beta(t) := \mu_{21}(t)$, where we assume $\beta(t) = f(v(t))$ for some function $f\in C^\infty(\mathbb{R})$ such that $f(0) = 0$ and $f \geq 0$. The requirement that $f(0) = 0$ is physically justified by the fact that the volume distribution stops evolving as soon as the convection vanishes, and therefore the diffusion has to vanish as well. The condition $f\geq 0$ is needed to avoid backward diffusion in the case the convection velocity v becomes negative. Indeed, as it becomes clearer in the following, this may happen when the nucleation rate "beats" the grain growth, and thus "drags" the volume distribution profile towards the left. Here, we choose $f(v) = \beta_1 v^2$, where $\beta_1 > 0$; however, in Section 4.2, we show the appearance of infinite-time blow-up if we violate the condition $f(0) = 0$ for the special case $f(v) = \beta_0 + \beta_1 v^2$ with $\beta_0 > 0$. All in all, the volume distribution ϕ satisfies the Fokker-Planck equation

$$\begin{cases} \phi_t = -v(t)(\nu\phi)_\nu + \beta_1 v(t)^2(\nu^2\phi)_{\nu\nu}, \\ \phi(\nu,t_0) = \phi_0(\nu), \end{cases} \quad \text{for all } (\nu,t)\in(0,\infty)\times(t_0,T], \tag{3.3}$$

where $\phi_0\in C^0(0,\infty)\cap L^\infty(0,\infty)$ is a probability density.

For any $n\geq 0$, we denote by $M_n(t) := \int_0^\infty \nu^n\phi(\nu,t)\,\mathrm{d}\nu$ (respectively $M_n^0 := M_n(t_0)$), the nth moment of ϕ, a solution to (3.3) (respectively ϕ_0, the initial profile). We compute

$$\begin{aligned} M_n'(t) &= \int_0^\infty \nu^n\phi_t(\nu,t)\,\mathrm{d}\nu = -v(t)\int_0^\infty \nu^n(\nu\phi)_\nu(\nu,t)\,\mathrm{d}x + \beta(t)\int_0^\infty \nu^n(\nu^2\phi)_{\nu\nu}(\nu,t)\,\mathrm{d}\nu \\ &= nv(t)\int_0^\infty \nu^n\phi(\nu,t)\,\mathrm{d}\nu - n\beta(t)\int_0^\infty \nu^{n-1}(\nu^2\phi)_\nu(\nu,t)\,\mathrm{d}\nu \\ &= nv(t)\int_0^\infty \nu^n\phi(\nu,t)\,\mathrm{d}\nu + n(n-1)\beta(t)\int_0^\infty \nu^n\phi(\nu,t)\,\mathrm{d}\nu = (nv(t)+n(n-1)\beta(t))M_n(t), \end{aligned}$$

where we implicitly need that

$$\begin{cases} \lim_{\nu\to 0} \nu^{n+1}\phi(\nu,t) = \lim_{\nu\to+\infty} \nu^{n+1}\phi(\nu,t) = 0, \\ \lim_{\nu\to 0} \nu^{n+2}\phi_\nu(\nu,t) = \lim_{\nu\to\infty} \nu^{n+2}\phi_\nu(\nu,t) = 0, \end{cases} \tag{3.4}$$

in order to carry out the integrations by parts. This gives

$$M_n(t) = M_n^0 \exp(nw(t) + n(n-1)b(t)) \quad \text{for all } t \in [t_0, T], \tag{3.5}$$

where $w(t) := \int_{t_0}^t v(s)\,\mathrm{d}s$ and $b(t) := \int_{t_0}^t \beta(s)\,\mathrm{d}s = \beta_1 \int_{t_0}^t v(s)^2\,\mathrm{d}s$. Now, from (3.2), we have $M_1(t) = g(t)$. Then, by (3.5), $g(t) = g_0 \exp(w(t))$, where $g_0 := g(t_0)$, which leads to

$$v(t) = \frac{g'(t)}{g(t)} = (\log \circ g)'(t) \quad \text{for all } t \in [t_0, T]. \tag{3.6}$$

Equation (3.6) tells us that the convection velocity v (and therefore the diffusion coefficient β, up to the multiplicative constant β_1) is determined by the evolution of the macroscopic quantity g given to us by the model in Section 2. We can also see the convection velocity as a measure for the evolution of g. We see again here the link between the meso- and macroscopic scales.

From (3.5) we can deduce that if t_0 was taken to be zero, i.e., ϕ_0 was a Dirac mass at the origin, then any solution to (3.3) would be ϕ_0 for all times, that is, nothing would happen. This reflects the existence of the incubation time $t_0 > 0$ before which we are unable to describe the behaviour of the volume distribution.

3.2. **A solution formula for the volume distribution.** We now derive an explicit solution for the Fokker-Planck equation (3.3). We introduce the transformation of variables

$$\begin{aligned} \xi &:= \log(\nu) + b(t) - w(t), \\ \tau &:= b(t), \\ h(\xi,t) &:= \nu\phi(\nu,t), \end{aligned}$$

with $h(\xi,\tau)\colon \mathbb{R} \times [0, b(T)] \to [0,\infty)$. The fact that b is non-decreasing allows us to introduce the time change of variables $\tau = b(t)$; this justifies the requirement that $f \geq 0$ in $\beta(t) = f(v(t))$ from a mathematical viewpoint. We see that $h(\xi,\tau)$ is governed by the linear heat equation

$$\begin{cases} h_\tau = h_{\xi\xi}, \\ h(\xi,0) = \mathrm{e}^\xi \phi_0(\mathrm{e}^\xi), \end{cases} \quad \text{for all } (\xi,\tau) \in \mathbb{R} \times (0, b(T)].$$

It is well-known that h is given by

$$h(\xi,\tau) = (K(\cdot,\tau) * \Phi_0)(\xi) \quad \text{for all } (\xi,\tau) \in \mathbb{R} \times (0, b(T)],$$

where $*$ is the convolution and

$$K(\xi,\tau) = (4\pi\tau)^{-1/2} \exp\left(-\xi^2/(4\tau)\right) \quad \text{and} \quad \Phi_0(\xi) = \mathrm{e}^\xi \phi_0(\mathrm{e}^\xi).$$

Transforming back to the original variables ν and t we finally obtain

$$\phi(\nu,t) = \nu^{-1}(K(\cdot, b(t)) * \Phi_0)(\log(\nu) + b(t) - w(t)) \quad \text{for all } (\nu,t) \in (0,\infty) \times (t_0, T]. \tag{3.7}$$

We now see that the resulting solution is a convolution of the initial distribution with a log-normal fundamental solution, which is what we expect from experiments [18]. This justifies the choice of the mobility terms in the Fokker-Planck equation (3.3) made earlier.

Note that the decay conditions (3.4) are satisfied for the solution in (3.7) if $M_{n+1}^0 < \infty$, see [19, Proposition 3.4]. Thus, the moments relation (3.5) holds when M_{n+1}^0 is finite—in particular, (3.6) holds when M_2^0 is finite. Also, by [19, Propositions 3.1 and 3.2], we have that ϕ as defined in (3.7) satisfies $\phi(\nu,t) \to \phi_0(\nu)$ as $t \to t_0$ for all $\nu \in (0,\infty)$ and $\phi \in C^{\infty,0}((0,\infty) \times [t_0,\infty))$.

Remark 3.1. If one assumes that grains do not have the time to touch each other or the boundary (for example if the final time is very small, or if the nucleation and growth rates are very small), and thus are exact, non-intersected spheres, then one may equivalently employ the *radius distribution* ψ in place of the volume distribution ϕ. The radius distribution

$$\psi(r,t)\colon (0,\infty)\times[t_0,T]\to[0,\infty)$$

counts, at time t, the number of grains of radius r per unit radius, normalised by the total number of grains, which leads, as for the volume distribution, to $\psi(\cdot,t)$ being a probability density on $(0,\infty)$. Since grains are spheres, there is a direct one-to-one relation between ϕ and ψ as the map $a\colon[0,\infty)\to[0,\infty), r\mapsto 4\pi r^3/3$, is a bijection. Indeed, this implies that, for all $r_2>r_1\geq 0$,

$$\int_{r_1}^{r_2}\psi(r,t)\,\mathrm{d}r=\int_{a(r_1)}^{a(r_2)}\phi(\nu,t)\,\mathrm{d}\nu=\int_{r_1}^{r_2}\phi(a(r),t)a'(r)\,\mathrm{d}r=\int_{r_1}^{r_2}\phi\left(\frac{4\pi r^3}{3},t\right)4\pi r^2\,\mathrm{d}r,$$

by a simple change of variable $x\longrightarrow a(r)$. This equality being true for all $r_2>r_1\geq 0$, we get

$$\psi(r,t)=4\pi r^2\phi\left(\tfrac{4\pi}{3}r^3,t\right)\quad\text{for all } r\in(0,\infty).$$

From the inverse transformation, one gets

$$\phi(\nu,t)=(4\pi)^{-1/3}(3\nu)^{-2/3}\psi\left(\left(\tfrac{3\nu}{4\pi}\right)^{1/3},t\right)\quad\text{for all } \nu\in(0,\infty).$$

Relation (3.2) then becomes

$$g(t)=\frac{4\pi}{3}\int_0^\infty r^3\psi(r,t)\,\mathrm{d}r.$$

4. Numerical simulations

In this section, we study the general qualitative behaviour of the model derived in Section 2 and the Fokker-Planck equation (3.3). As initial distribution we take the log-normal profile

$$\phi_0(\nu)=(\nu\sigma_0\sqrt{2\pi})^{-1}\exp(-(\log(\nu)-\mu_0)^2/(2\sigma_0^2))\quad\text{for all } \nu\in(0,\infty),$$

with $\mu_0=\log(g_0)-\sigma_0^2/2$; in fact, $g_0=M_1^0=\exp(\mu_0+\sigma_0^2/2)$. The standard variation σ_0 cannot be extracted from the model in Section 2 (as is g_0), and is therefore an additional parameter. Unless mentioned otherwise, the simulations below approximate (2.4) and plot (3.7) for the parameters

$$\rho_*=1,\quad P^{\mathrm{eq}}=0.45,\quad \alpha=0.001,\quad \gamma=0.5,\quad \beta_1=0.01,\quad t_0=0.3387,\quad \sigma_0=0.4.$$

The value of t_0 is arbitrary and is only chosen as above for convenience in the following simulations.

4.1. The main quantities.

From Figures 1a and 1b, we can see that the quantities $g(t)$ and $P(t)$ are sigmoid functions, reaching "quickly" values close to their equilibrium. The evolution of the log-normal volume distribution of ferrite grains $\phi(\cdot,t)$ is given in Figure 1c.

4.2. Infinite-time blow-up.

We observe here the behaviour of the solution ϕ when the condition $f(0)=0$ is violated in $\beta(t)=f(v(t))$ in the special case $f(v)=\beta_0+\beta_1 v^2$ for $\beta_0=0.005$. Since g goes to an equilibrium value as t increases and $v=g'/g$ by (3.6), then v tends to 0 (if g does not oscillate around its equilibrium value). Therefore $f(v(t))$ tends to $\beta_0\neq 0$ as t increases, and the Fokker-Planck equation (3.3) formally becomes

$$\phi_t=\beta_0(\nu^2\phi)_{\nu\nu},$$

which blows up in infinite time, as illustrated in Figure 2.

From Figure 2a, the solution first drifts to the right, until the diffusion takes over and makes the solution drift to the left. Infinite-time blow-up occurs, see Figure 2b.

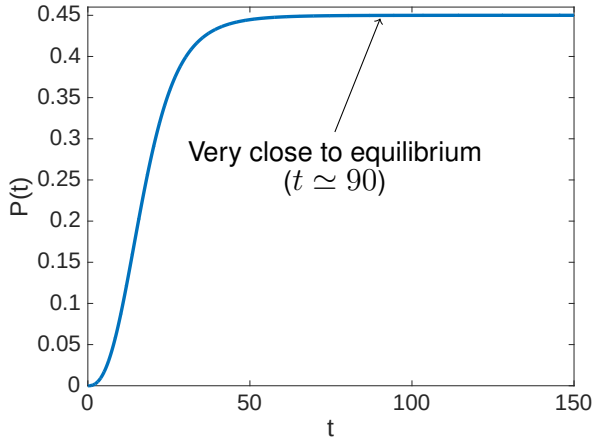

(a) Evolution of $P(t)$

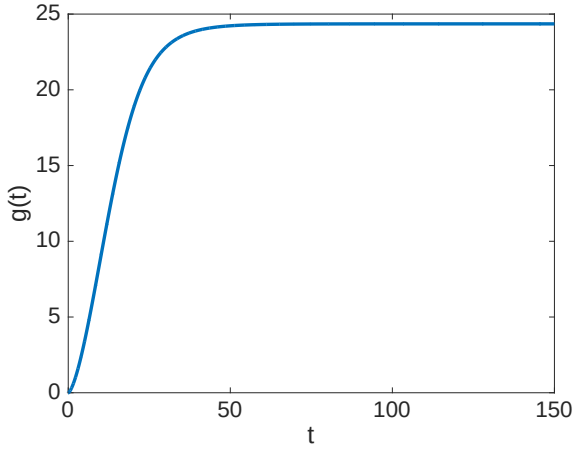

(b) Evolution of $g(t) := P(t)/N(t)$

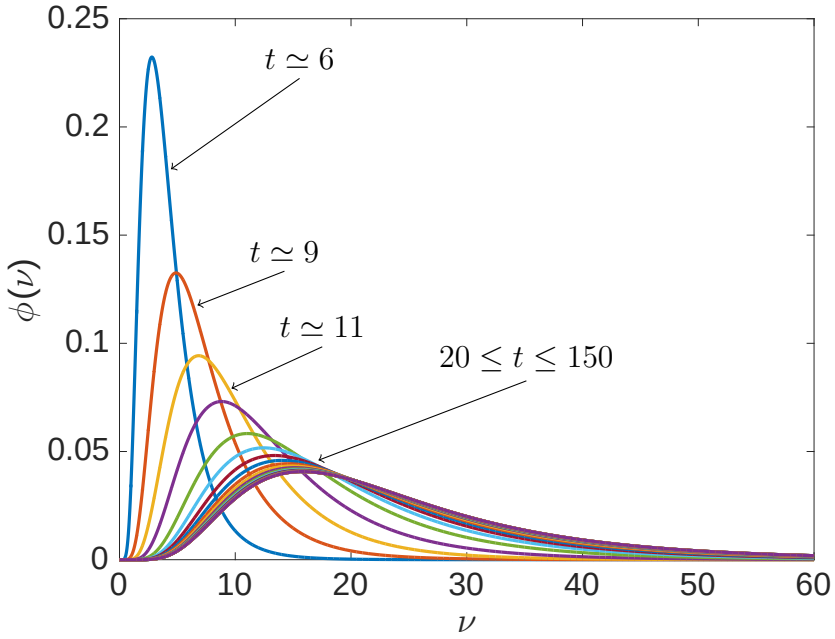

(c) Evolution of $\phi(\cdot, t)$ up to $t = 150$

FIGURE 1. Evolution of the main quantities.

4.3. **Parameter study.** Figures 3a and 3b show that the effect of increasing the reference growth rate ρ_* or the equilibrium phase fraction P^{eq} turns out to be to make the profile flat and drift to the right more quickly. The effect of increasing the nucleation rate α or the power γ is the opposite, see Figures 3c and 3d. Increasing the diffusion coefficient β_1 or the initial standard deviation σ_0 makes the solution flatten and shift to the left, as shown in Figures 3e and 3f.

In Figures 4a, 4b and 4c, one sees that the effect of increasing ρ_*, P^{eq} or α is to make the solution approach the equilibrium faster. Figure 4d shows that increasing γ has the contrary effect.

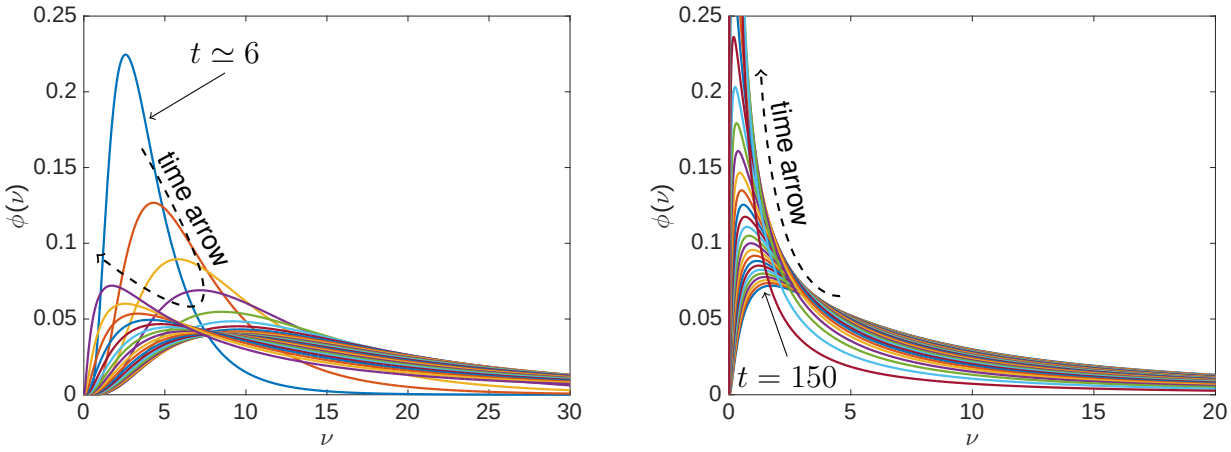

(a) Solution up to $t = 150$

(b) Solution up to $t = 1000$

FIGURE 2. Volume distribution for $\beta_0 = 0.005$.

5. VOLUME AND AREA DISTRIBUTIONS: RELATION BETWEEN MODEL AND EXPERIMENTS

To validate our grain-size model, the resulting volume distribution has to be related to experimental data which are typically derived from a two-dimensional micrograph section, under the form of an area distribution. We here derive a relationship between these two distributions which can pave the way to a quantitative validation with measurements in a forthcoming paper. We point out that the following derivation only holds in the setting of Remark 3.1; we therefore equivalently deal with three-dimensional and two-dimensional radius distributions instead of volume and area distributions, respectively.

We follow the approach of [15] and consider a cylindrically shaped steel specimen Ω with base area q, axially symmetric to the z-axis and of length $L \gg \sqrt{q/\pi}$. We want to relate the spherical grains in Ω with their two-dimensional counterparts, that is, with the discs resulting from the intersection of the spherical grains with the plane $\{z = 0\}$. Let us fix a time t, and define $\chi(\eta, t)$ as the number of such intersection discs with radius η per unit radius per unit surface. (Note that, unlike ψ, χ is not normalised by the total number of circular grains (intersection discs) in the cross-section $\Omega \cap \{z = 0\}$, but it is rather a quantity per unit surface.) Due to the boundedness of the test specimen, we may assume that the radius of the spherical grains is bounded by some $r_{\max} \leq \sqrt{q/\pi}$, so that $0 \leq \eta \leq r_{\max}$. Now let us choose $\eta \in [0, r_{\max})$ and $\Delta\eta > 0$ small. Then the number of circular grains in the cross-section with radii in $[\eta, \eta + \Delta\eta]$ is given by $q \int_\eta^{\eta+\Delta\eta} \chi(\zeta, t)\, \mathrm{d}\zeta$. To relate this to ψ, we fix $\Delta r > 0$ small and, for any spherical grain radius $r \in [\eta + \Delta\eta, r_{\max} - \Delta r]$, we infer that the centres of the spherical grains in the right part of the cylindrical specimen (i.e., in $\Omega \cap \{z \geq 0\}$) with radii in $[r, r + \Delta r]$ creating intersection discs with radii in $[\eta, \eta + \Delta\eta]$ lie in an interval $[\tilde{z}, \tilde{z} + \delta]$, as shown in Figure 5.

Note that δ depends on $\eta, \Delta\eta, r$ and Δr; also, for $r = \eta + \Delta\eta$, we have $\tilde{z} = 0$. As it is immediate from Figure 5, we have

$$\delta = \delta(r) = \sqrt{(r + \Delta r)^2 - \eta^2} - \sqrt{r^2 - (\eta + \Delta\eta)^2}. \tag{5.1}$$

Now we choose $n \in \mathbb{N}$, define $\Delta r = (r_{\max} - (\eta + \Delta\eta))/n$ and introduce the equi-spaced partition

$$r_i = \eta + \Delta\eta + i\Delta r, \quad 0 \leq i \leq n,$$

and accordingly $\delta_i = \delta(r_i)$, see (5.1). A first order Taylor expansion yields

$$\delta_i = c_i\eta\Delta\eta + c_i r_i \Delta r + o(\Delta\eta) + o(\Delta r),$$

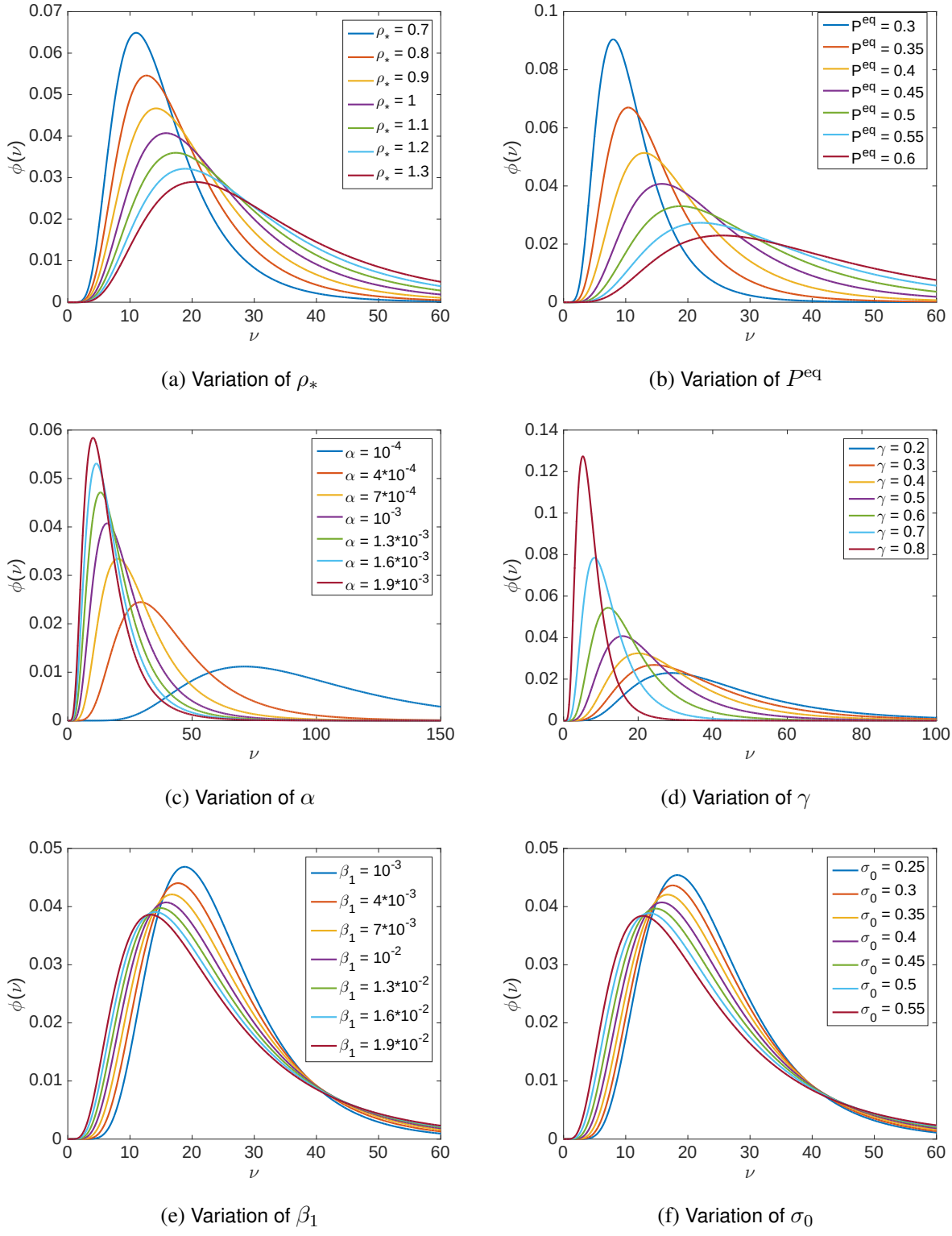

(a) Variation of ρ_*

(b) Variation of P^{eq}

(c) Variation of α

(d) Variation of γ

(e) Variation of β_1

(f) Variation of σ_0

FIGURE 3. Volume distribution at $t = 150$ for different parameter variations.

with $c_i := (r_i^2 - \eta^2)^{-1/2}$. Note that, by the boundedness of r_i, the terms $o(\Delta\eta)$ and $o(\Delta r)$ in the above formula are uniform in i. In the limit $\Delta r \to 0$, for any $0 \le i \le n-1$, the total number of spherical grains in $\Omega \cap \{z \ge 0\}$ with radii in $[r_i, r_{i+1}]$ contributing to circular grains in the cross-section with radii in $[\eta, \eta + \Delta\eta]$ is $N(t) q \delta_i \int_{r_i}^{r_{i+1}} \psi(r,t)\,\mathrm{d}r$, with $N(t)$ being the number of ferrite grains per unit volume given in (2.5). We sum over all transversal cylindrical pieces of Ω with volumes $q\delta_i$, accounting also for

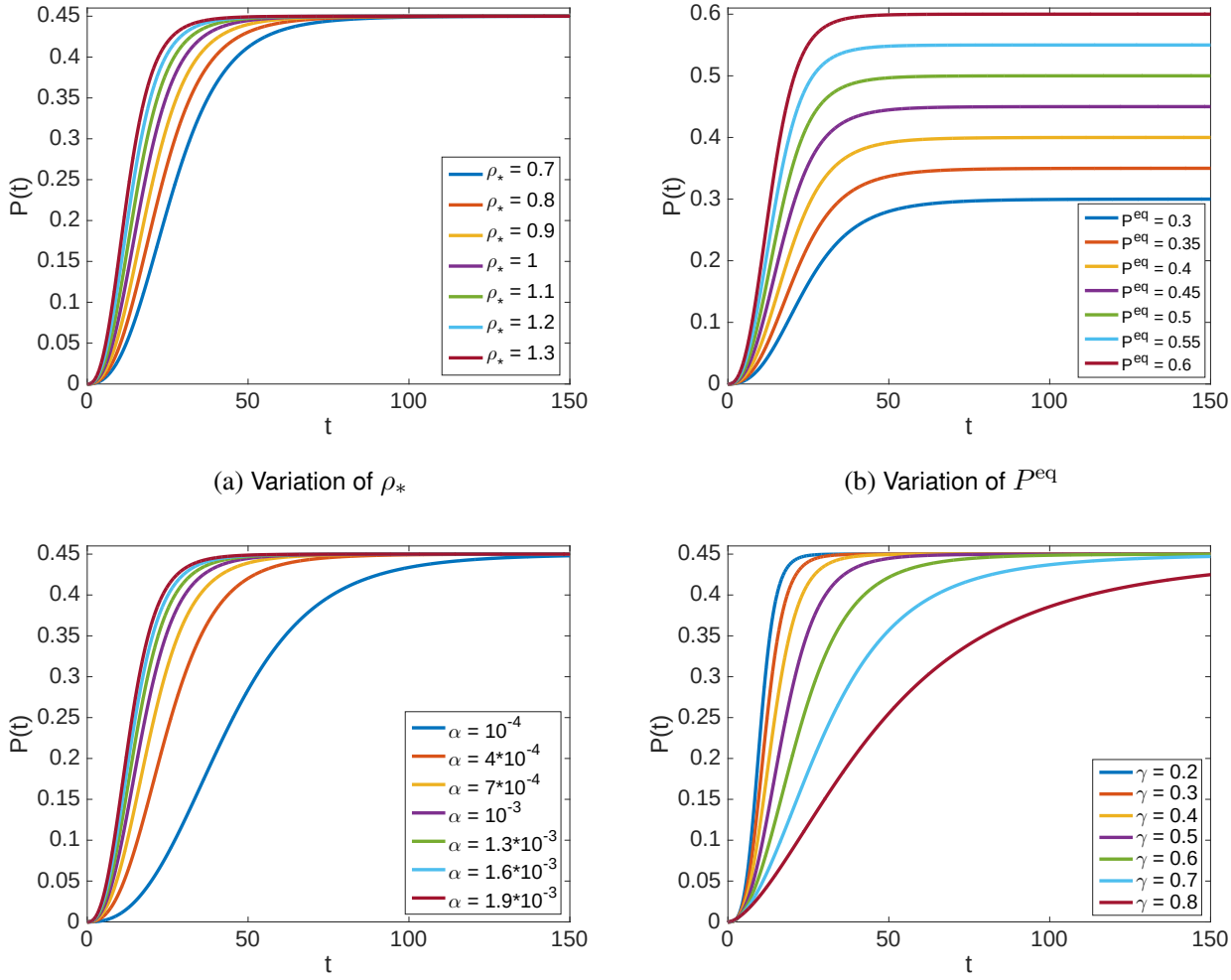

(a) Variation of ρ_*

(b) Variation of P^{eq}

(c) Variation of α

(d) Variation of γ

FIGURE 4. Ferrite volume phase fraction at $t = 150$ for different parameter variations.

those in the left part of the specimen $\Omega \cap \{z \leq 0\}$ (hence, by symmetry, the factor 2 in the computation below), and use the boundedness of ψ and ψ_r to obtain

$$\begin{aligned} q\int_{\eta}^{\eta+\Delta\eta} \chi(\zeta,t)\,\mathrm{d}\zeta &= 2N(t)q\sum_{i=0}^{n-1}\delta_i\int_{r_i}^{r_{i+1}}\psi(r,t)\,\mathrm{d}r + O(\Delta r)\\ &= 2N(t)q\sum_{i=0}^{n-1}\delta_i\Big(\Delta r\psi(r_i,t)+o(\Delta r)\Big)+O(\Delta r)\\ &= 2N(t)q\sum_{i=0}^{n-1}\Big(c_i\eta\Delta\eta + c_i r_i\Delta r + o(\Delta\eta)+o(\Delta r)\Big)\Big(\Delta r\psi(r_i,t)+o(\Delta r)\Big)+O(\Delta r)\\ &= 2N(t)q\sum_{i=0}^{n-1}\frac{\psi(r_i,t)\eta\Delta\eta\Delta r}{\sqrt{r_i^2-\eta^2}}+o(\Delta\eta)+O(\Delta r). \end{aligned}$$

By letting $\Delta r \to 0$ in the above computation, we get

$$q\int_{\eta}^{\eta+\Delta\eta}\chi(\zeta,t)\,\mathrm{d}\zeta = 2N(t)q\int_{\eta+\Delta\eta}^{r_{\max}}\frac{\eta\Delta\eta\psi(r,t)}{\sqrt{r^2-\eta^2}}\,\mathrm{d}r + o(\Delta\eta).$$

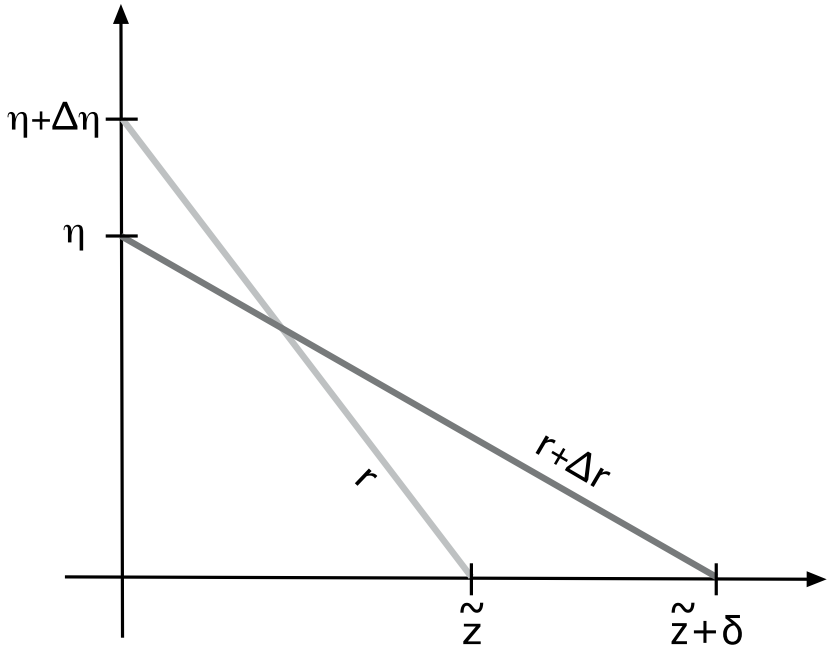

FIGURE 5. Position of spherical grain centres in right half of specimen.

Then, dividing by $q\Delta\eta$ and passing to the limit with $\Delta\eta \to 0$, we finally obtain

$$\chi(\eta,t) = 2N(t)\eta \int_{\eta}^{r_{\max}} \frac{\psi(r,t)}{\sqrt{r^2-\eta^2}}\,\mathrm{d}r \quad \text{for all } \eta \in (0, r_{\max}]. \tag{5.2}$$

This equation relates the three-dimensional radius distribution of a given specimen to the two-dimensional one in a cross-section of this specimen; note that this is independent of the area q of the cross-section. In Figure 6 we give an example of comparison between ψ and χ for $r_{\max} = 3$, according to (5.2). (Note that, in Figure 6, ψ and χ are appropriately normalised to have unit mass on $(0, r_{\max}]$.)

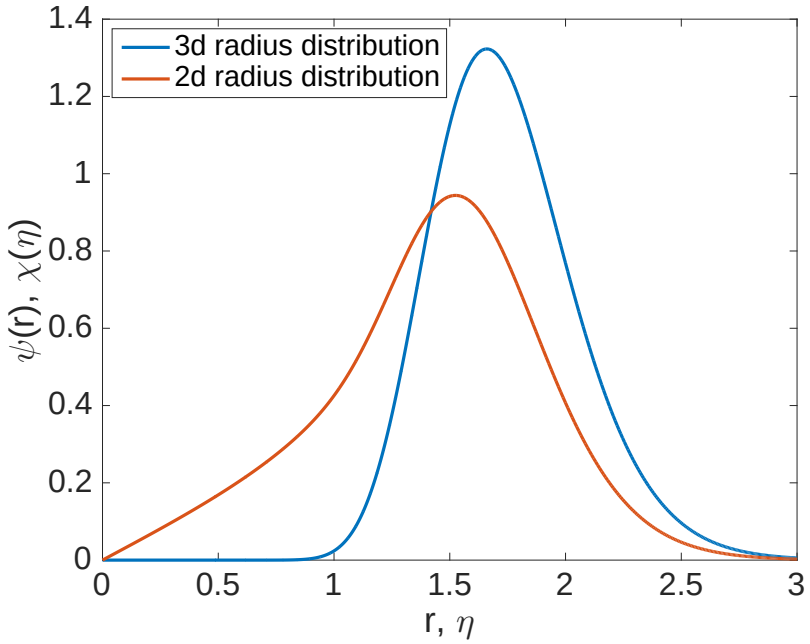

FIGURE 6. Three-dimensional radius distribution against two-dimensional one.

Let us finally point out that an easy calculation shows that the surface fraction of ferrite over the cross-section actually coincides with its volume fraction in the specimen. Call P_{s} the surface fraction of ferrite, i.e., the total surface of ferrite present on the cross-section normalised by q, and use formula (5.2) to get, for all $t \in [t_0, T]$,

$$P_{\mathrm{s}}(t) = \pi \int_0^{r_{\max}} \eta^2 \chi(\eta, t)\, \mathrm{d}\eta = 2\pi N(t) \int_0^{r_{\max}} \eta^3 \int_\eta^{r_{\max}} \frac{\psi(r,t)}{\sqrt{r^2-\eta^2}}\, \mathrm{d}r\, \mathrm{d}\eta$$

$$= 2\pi N(t) \int_0^{r_{\max}} \psi(r,t) \underbrace{\left(\int_0^r \frac{\eta^3}{\sqrt{r^2-\eta^2}}\, \mathrm{d}\eta \right)}_{=2r^3/3} dr = \frac{4\pi N(t)}{3} \int_0^{r_{\max}} r^3 \psi(r,t)\, \mathrm{d}r = P(t).$$

Acknowledgements. D. Hömberg gratefully acknowledges a sabbatical stay at the University of Bath where the research that led to this work was initiated. J. Zimmer gratefully acknowledges partial funding by the EPSRC through project EP/K027743/1, the Leverhulme Trust, RPG-2013-261, and a Royal Society Wolfson Research Merit Award.

REFERENCES

[1] M. Avrami. Kinetics of phase change. I General theory. *J. Chem. Phys.*, 7(12):1103–1112, 1939.

[2] M. Avrami. Kinetics of phase change. II TransformationIJôòðtime relations for random distribution of nuclei. *J. Chem. Phys.*, 8(12):212–224, 1940.

[3] M. Avrami. Kinetics of phase change. III Granulation, phase change, and microstructure. *J. Chem. Phys.*, 9(2):177–184, 1941.

[4] J. M. Ball, J. Carr, and O. Penrose. The Becker-Döring cluster equations: basic properties and asymptotic behaviour of solutions. *Comm. Math. Phys.*, 104(4):657–692, 1986.

[5] K. Barmak, E. Eggeling, M. Emelianenko, Y. Epshteyn, D. Kinderlehrer, R. Sharp, and S. Ta'asan. Critical events, entropy, and the grain boundary character distribution. *Phys. Rev. B*, 83:134117, Apr 2011.

[6] K. Barmak, E. Eggeling, M. Emelianenko, Y. Epshteyn, D. Kinderlehrer, R. Sharp, and S. Ta'asan. Predictive theory for the grain boundary character distribution. *Mater. Sci. Forum*, 715-716:279–285, 2012.

[7] S. Berbenni, V. Favier, and M. Berveiller. Impact of the grain size distribution on the yield stress of heterogeneous materials. *Int. J. Plasticity*, 23(1):114 – 142, 2007.

[8] W. Bleck, D. Hömberg, U. Prahl, P. Suwanpinij, and N. Togobytska. Optimal control of a cooling line for production of hot rolled dual phase steel. *Steel Res. Int.*, 85(9):1328–1333, 2014.

[9] E. A. Carlen and W. Gangbo. Constrained steepest descent in the 2-Wasserstein metric. *Ann. of Math. (2)*, 157(3):807–846, 2003.

[10] S. Cordier, L. Pareschi, and C. Piatecki. Mesoscopic modelling of financial markets. *J. Stat. Phys.*, 134(1):161–184, 2009.

[11] W. Dreyer, R. Huth, A. Mielke, J. Rehberg, and M. Winkler. Global existence for a nonlocal and nonlinear Fokker-Planck equation. *Z. Angew. Math. Phys.*, 66(2):293–315, 2015.

[12] M. Fanfoni and M. Tomellini. The Johnson-Mehl-Avrami-Kohnogorov model: A brief review. *Il Nuovo Cimento D*, 20(7):1171–1182, 1998.

[13] D. Hömberg, S. Lu, K. Sakamoto, and M. Yamamoto. Parameter identification in non-isothermal nucleation and growth processes. *Inverse Problems*, 30(3):035003, 24, 2014.

[14] D. Hömberg, N. Togobytska, and M. Yamamoto. On the evaluation of dilatometer experiments. *Appl. Analysis*, 88:669–681, 2009.

[15] A. Huber. Zur Kinetik von Kristallisationsvorgängen. *Zeitschrift für Physik*, 93(3):227–231, 1935.

[16] W. A. Johnson and R. F. Mehl. Reaction kinetics in processes of nucleation and growth. *Trans. Am. Inst. Min. Metall. Eng.*, 135:416–442, 1939.

[17] A. N. Kolmogorov. On the statistical theory of metal crystallization. *Izv. Akad. Nauk SSSR Ser. Mat.*, pages 355–360, 1937.

[18] M. Militzer, E. B. Hawbolt, T. Ray Meadowcroft, and A. Giumelli. Austenite grain growth kinetics in Al-killed plain carbon steels. *Metall. Mater. Trans. A*, 27(11):3399–3409, 1996.

[19] F. S. Patacchini. Evolution of the grain size distribution in steel. *MSc Thesis, University of Bath*, 2013. Available at http://www.bath.ac.uk/library/dissertations/index.php?programme=MSc+Modern+Applications+of+Mathematics&online=.

[20] O. Penrose. Metastable states for the Becker-Döring cluster equations. *Comm. Math. Phys.*, 124(4):515–541, 1989.

[21] P. Suwanpinij, N. Togobytska, U. Prahl, W. Weiss, D. Hömberg, and W. Bleck. Numerical cooling strategy design for hot rolled dual phase steel. *Steel Res. Int.*, 81:1001–1009, 2010.

[22] G. E. Totten and M. A. H. Howes. *Steel Heat Treatment Handbook*. CRC Press, 2nd edition, 1997.

[23] A. Tudorascu and M. Wunsch. On a nonlinear, nonlocal parabolic problem with conservation of mass, mean and variance. *Comm. Partial Differential Equations*, 36(8):1426–1454, 2011.